AIAA JOURNAL
Vol. 49, No. 7, July 2011

Aeroacoustic Integrals Accelerated by Fast Multipole Method

William R. Wolf and Sanjiva K. Lele
Stanford University, Stanford, California 94305-4035

DOI: 10.2514/1.J050861

The calculation of acoustic field solutions due to aeroacoustic sources is performed for a large number of observer locations. Sound is predicted by a hybrid method that uses direct calculation for near-field source computations and the Ffowcs Williams–Hawkings equation as the acoustic analogy formulation. The integrations of surface dipole and volume quadrupole source terms appearing in the Ffowcs Williams–Hawkings formulation are accelerated by a three-dimensional wideband multilevel adaptive fast multipole method. The three-dimensional wideband fast multipole method presented here applies a plane-wave expansion formulation with fast spherical filtering and interpolation and diagonal translation for calculations in the high-frequency regime and a partial-wave expansion formulation with rotational–coaxial translation in the low-frequency regime. The method is described for the solution of a three-dimensional Green's function that incorporates convective effects. The sound generated by the unsteady flow past a cylinder in the proximity of a NACA0012 airfoil is studied and the interaction of both geometries is analyzed for different cylinder positions. The developed numerical capability allows the analysis of each noise source individually. Therefore, the effects of dipoles and quadrupoles for each configuration are investigated. Results for acoustic field solutions obtained by the accelerated Ffowcs Williams–Hawkings formulation are up to 2 orders of magnitude faster than with the conventional computation of Ffowcs Williams–Hawkings equation.

Nomenclature

c_0 = speed of sound
$D(.)$ = diagonal operator in plane-wave expansion formulation
F_i = dipole source
f = Ffowcs Williams–Hawkings surface
G = Green's function
H = Heaviside function
$h_n^{(2)}$ = spherical Hankel function of the second kind and order n
$I(.)$ = plane-wave operator in plane-wave expansion formulation
i = imaginary unit
j_n = spherical Bessel function of the first kind and order n
K = modified wave number
k = wave number
$L(.)$ = local expansion in the fast multipole method
M = Mach number
$M(.)$ = multipole expansion in the fast multipole method
P_n = Legendre polynomial of degree n
P_n^m = associated Legendre polynomial of degree n and order m
p = pressure
Q = monopole source
$R(.)$ = regular operator in partial-wave expansion formulation
St = Strouhal number
$S(.)$ = singular operator in partial-wave expansion formulation
T_{ij} = quadrupole source (Lighthill stress tensor)
U_i = freestream velocity vector
X_i = observer location in transformed coordinates
x_i = observer location
Y_i = source location in transformed coordinates
y_i = source location
ω = angular frequency

I. Introduction

THE development of physics-based noise-prediction tools for analysis of aerodynamic noise sources is of paramount importance, since noise regulations have become more stringent. Therefore, more sophisticated methods are needed to achieve the required noise reductions without a significant performance penalty. The design of 3-D realistic configurations requires the use of time-consuming numerical simulations for the study and mitigation of jet, fan, and airframe noise sources. Direct simulation of noise remains prohibitively expensive for engineering problems because of resolution requirements. Therefore, hybrid approaches that consist of predicting near-field flow quantities by a suitable computational fluid dynamics (CFD) simulation and far-field sound radiation by aeroacoustic integral methods, e.g., acoustic analogy formulations, are more attractive. The flow physics associated with sound generation must be accurately captured in the CFD calculation in order to be used in this context. A literature review of integral formulations applied in the context of hybrid methods is presented in [1] for aeroacoustic applications.

For design purposes, it is important to compute acoustic field solutions in order to understand the interaction between noise sources and complex aerodynamic configurations, including scattering and diffraction of sound waves by multiple geometries that may contain sharp corners and cavities, for example. Moreover, spherically resolved directivity mappings may be required for the study of far-field noise radiated from realistic 3-D configurations. Two examples that can be cited in this context are those of airliners during airport landing operations or any situation in which an aircraft is required to maneuver relatively close to the ground. Because flyovers of some duration are involved in both cases, a desirable prediction output could be that of a lower hemisphere in the acoustic far field that is densely populated with observers.

The computation of acoustic field solutions and spherically resolved directivity mappings requiring many observer locations presents a high computational cost. In [2], a numerical method is presented for fast computation of sound field solutions at many observer locations and it is applied to the study of a jet noise problem. However, as discussed by the author, the method is expensive for far-field calculations and does not address convective effects. In [3,4], numerical methods are presented for the fast computation of acoustic fields for 2-D aeroacoustic problems in the time and frequency domains, respectively. Each method has advantages and drawbacks that are dependent on the application. While time-domain formulations are the natural choice for problems with nonperiodic sound

---

Received 11 August 2010; revision received 7 December 2010; accepted for publication 12 December 2010.

[*] Ph.D. Candidate, Department of Aeronautics and Astronautics. Member AIAA.

[†] Professor, Department of Aeronautics and Astronautics; Department of Mechanical Engineering.

generation, frequency-domain formulations require simpler implementation and can provide sound data for specific frequencies of interest. In addition to these differences, Lockard [5] shows that frequency-domain methods present lower computational cost than with time-domain methods, even when multiple frequencies are analyzed.

In this work, the authors extend the formulation presented in [4] for the solution of 3-D aeroacoustic problems. The sound generated by the unsteady flow past a cylinder in the proximity of a NACA0012 airfoil is studied and the interaction of both geometries is analyzed for different cylinder positions. The developed numerical capability allows the analysis of each noise source individually. Therefore, it is possible to investigate the effects of dipole and quadrupole sources for each configuration and the effects of convection on the computation of noise radiated by these sources. To reduce the computational cost of field solutions at many observer locations, the integrations of surface dipole and volume quadrupole source terms are accelerated by a 3-D wideband multilevel adaptive fast multipole method [6] (FMM). The 3-D wideband FMM presented here applies a plane-wave expansion formulation [7,8] with fast spherical filtering and interpolation [9] and diagonal translation for calculations in the high-frequency regime and a partial-wave expansion formulation [10] with rotational–coaxial translation [11] in the low-frequency regime. The method is described for the solution of a 3-D Green's function that incorporates convective effects [5,12].

With the acceleration provided by the method described in this paper, noise sources from CFD grids can be directly used for acoustic predictions. The method can be also applied to obtain fast solutions and fast incident field computations for boundary integral equation methods such as the boundary element method or the equivalent source method. The study of sound generated by landing gears and high-lift devices can benefit from the method developed here, since fast and accurate field solutions can be obtained for complex configurations.

II. Flow Simulations

The general curvilinear form of the compressible Navier–Stokes equations is solved using direct calculation of flows for low Mach and moderate Reynolds numbers. This direct calculation resolves the unsteady flow and the acoustic field generated by the flow. The numerical scheme for spatial discretization is a sixth-order-accurate compact scheme [13] implemented on a staggered grid. The current numerical capability allows the use of overset grids with a fourth-order-accurate Hermitian interpolation between grid blocks [14]. The time integration of the fluid equations is carried out by a fully implicit second-order Beam–Warming scheme [15] in the near-wall region in order to overcome the time-step restriction. A third-order Runge–Kutta scheme is used for time advancement of the equations in flow regions far away from solid boundaries. No-slip adiabatic wall boundary conditions are applied along the solid surfaces, and characteristic plus sponge boundary conditions are applied in the far-field locations. The numerical tool has been previously validated for several compressible flow simulations [14,16].

III. Acoustic Predictions

The Ffowcs Williams–Hawkings (FWH) [17] acoustic analogy formulation is used to predict the acoustic far fields radiated by the unsteady flow simulations. The FWH equation is applicable to bodies in arbitrary motion. However, in the present work, scattering bodies and observer locations are assumed to be in steady uniform motion in a stagnant medium. Following the development of Lockard [5], the FWH formulation for steady uniform motion can be written as

$$[\hat{p}'H(f)] = -\int_{f=0}\left[i\omega\hat{Q}(\mathbf{y})G(\mathbf{x},\mathbf{y}) + \hat{F}_i(\mathbf{y})\frac{\partial G(\mathbf{x},\mathbf{y})}{\partial y_i}\right]\mathrm{d}S - \int_{f>0}\hat{T}_{ij}H(f)\frac{\partial^2 G(\mathbf{x},\mathbf{y})}{\partial y_i \partial y_j}\,\mathrm{d}V \qquad (1)$$

where p' is the acoustic pressure, i is the imaginary unit, ω is the angular frequency, $f = 0$ represents the FWH surface, and $H(f)$ is the Heaviside function defined as $H(f) = 1$ for $f > 0$ and $H(f) = 0$ for $f < 0$. The monopole and dipole source terms are $Q = [\rho(u_i + U_i) - \rho_0 U_i]\partial f/\partial x_i$ and $F_i = [p\delta_{ij} - \tau_{ij} + \rho(u_i - U_i)(u_j + U_j) + \rho_0 U_i U_j]\partial f/\partial x_j$, respectively, and T_{ij} is the Lighthill stress tensor or quadrupole source term given by $T_{ij} = \rho u_i u_j + (p' - c_0^2\rho')\delta_{ij} - \tau_{ij}$. Here, c_0 is the speed of sound, u_i is the fluid velocity vector, U_i is the FWH surface velocity vector, p is the pressure, ρ_0 is the freestream density, δ_{ij} is the Kronecker delta, and τ_{ij} is the viscous stress tensor, whose effects are considered negligible for the acoustic problems analyzed in the present work.

In Eq. (1), the circumflex $\hat{}$ denotes a frequency-domain quantity. Considering a mean flow velocity in the x Cartesian direction, the 3-D Green's function that incorporates convective effects [12] is given by

$$G(\mathbf{x},\mathbf{y}) = -\frac{e^{-ik[\sqrt{(x_1-y_1)^2+(1-M^2)[(x_2-y_2)^2+(x_3-y_3)^2]}-M(x_1-y_1)]/(1-M^2)}}{4\pi\sqrt{(x_1-y_1)^2+(1-M^2)[(x_2-y_2)^2+(x_3-y_3)^2]}} \qquad (2)$$

In Eq. (2), k is the wave number, M is the freestream Mach number defined as $M \equiv U_1/c_0$, $\mathbf{x} = (x_1, x_2, x_3)^t$ is an observer location, and $\mathbf{y} = (y_1, y_2, y_3)^t$ is a source location.

In the present work, the surface integrations appearing in Eq. (1) are computed along the scattering body surfaces. Therefore, the monopole source terms are steady in time and do not appear in the frequency-domain formulation, and the dipole source terms are given by $\hat{F}_i = \hat{p}'n_i$. Here, n_i is the component of the outward unit normal vector in the i Cartesian direction. The volume integrations in Eq. (1) are computed along a subset region of the flowfield, including the wake-plus-boundary-layer regions, where the magnitude of quadrupole sources may be nonnegligible. Generally, for low-Mach-number flows, these volume integrals are neglected, since the effects of quadrupole source terms are small, compared with those of dipole and monopole sources. Furthermore, these calculations are computationally expensive, since large-volume regions containing millions of source terms have to be integrated in order to avoid the effects of eddies exiting from the source integration domain. Wang et al. [18] show that these escaping eddies generate spurious noise that may severely contaminate the acoustic field solution. They also develop a method to overcome this difficulty. However, for jet flows, quadrupole sources have to be computed, since they are the dominant noise sources, and for wake and shear-layer flows, quadrupole sources have an important contribution to noise generation. Casper et al. [19] show the contribution of quadrupole sources to the noise associated with a high-lift wing configuration. With the method presented in this work, the computational cost of these volume integrations is considerably reduced.

IV. Fast Multipole Method

In this work, the surface and volume integrations of dipole and quadrupole source terms are performed using a 3-D wideband multilevel adaptive FMM in order to accelerate the calculations. In the current context, the FMM consists of clustering noise sources from a CFD grid at different spatial lengths in multipole expansions and evaluating their effects at clusters of observer locations that are well separated from the noise sources. We define two well-separated clusters as sets of elements (sources and observers) that are circumscribed by spheres and whose centroids are distant from each other by a length of at least four times their radius.

In the FMM-FWH method, a cubical box surrounds a CFD grid containing surface and volume noise sources and an acoustic grid containing many observer locations. Then a recursive algorithm for the refinement of this box is applied in order to form the refinement levels of the multilevel FMM. The general idea consists of refining the box into eight smaller boxes and inspecting the number of sources and observers contained by each of the new boxes. This process continues until the number of elements inside all the boxes is smaller than, or equal to, a certain prescribed number. This prescribed number of elements per box will define the maximum refinement level in the FMM. Following an oct-tree algorithm, one can define sets of lists containing some specific boxes, such as boxes that share nodes or edges, well-separated boxes at the same level of refinement, and others. These lists will help with the computation of multipole and local expansions, including their translations and conversions. The authors refer the reader to the papers by Nishimura [20] and Wolf and Lele [6] for a review of the FMM algorithm and a complete description of the 3-D wideband FMM, respectively.

In the FMM-FWH method, instead of computing the influence of all source terms at y_i to all observer locations at x_j directly, one can first modify Eq. (2) and write it as

$$G(\mathbf{X},\mathbf{Y}) = -\frac{e^{-iK[\sqrt{(X_1-Y_1)^2+(X_2-Y_2)^2+(X_3-Y_3)^2}-M(X_1-Y_1)]}}{4\pi\sqrt{(X_1-Y_1)^2+(X_2-Y_2)^2+(X_3-Y_3)^2}} \quad (3)$$

where $K = k/(1-M^2)$, $\mathbf{X} = (x_1, \sqrt{1-M^2}x_2, \sqrt{1-M^2}x_3)^t$, and $\mathbf{Y} = (y_1, \sqrt{1-M^2}y_2, \sqrt{1-M^2}y_3)^t$. Then one can compute multipole approximations representing the acoustic field of clusters of noise sources at observer locations far away from these clusters. To achieve a good performance, the FMM requires several levels of refinement along the acoustic source region and observer locations. To avoid numerical instabilities [21] for low-frequency analysis and at high levels of refinement of the FMM, a wideband formulation is implemented [6]. In Fig. 1a, note the multiple levels of adaptive refinement surrounding the dipole source region and far-field location of the cylinder-plus-airfoil configuration studied in this work. Figure 1b shows a detail of the FMM refinement along the configuration. In Figs. 1c and 1d, note the 2-D views of the source and observer locations and a detail of the dipole source region, respectively.

The current 3-D wideband formulation applies a plane-wave expansion formulation [7,8] with fast spherical filtering and interpolation [9] and diagonal translation for calculations in the high-frequency regime and a partial-wave expansion formulation [10] with rotational–coaxial translation [11] in the low-frequency regime. The former formulation has a lower computational cost than the latter; however, it is unstable at low frequencies or at high levels of adaptive refinement of the FMM. The latter formulation is stable for all frequency ranges, but has a higher computational cost at high frequencies. In the plane-wave expansion method, Green's function from Eq. (3) is written as

$$G(\mathbf{X},\mathbf{Y}) = \frac{iK}{16\pi^2} e^{iMK(X_1-Y_1)} \oint I(\mathbf{oY},\mathbf{K}) D(\mathbf{oX},\mathbf{K})\,\mathrm{d}(\mathbf{K}/|\mathbf{K}|) \quad (4)$$

where the plane-wave operator is given by

$$I(\mathbf{oY},\mathbf{K}) = e^{-i\mathbf{K}\cdot\mathbf{oY}} \quad (5)$$

and the diagonal translation operator is given by

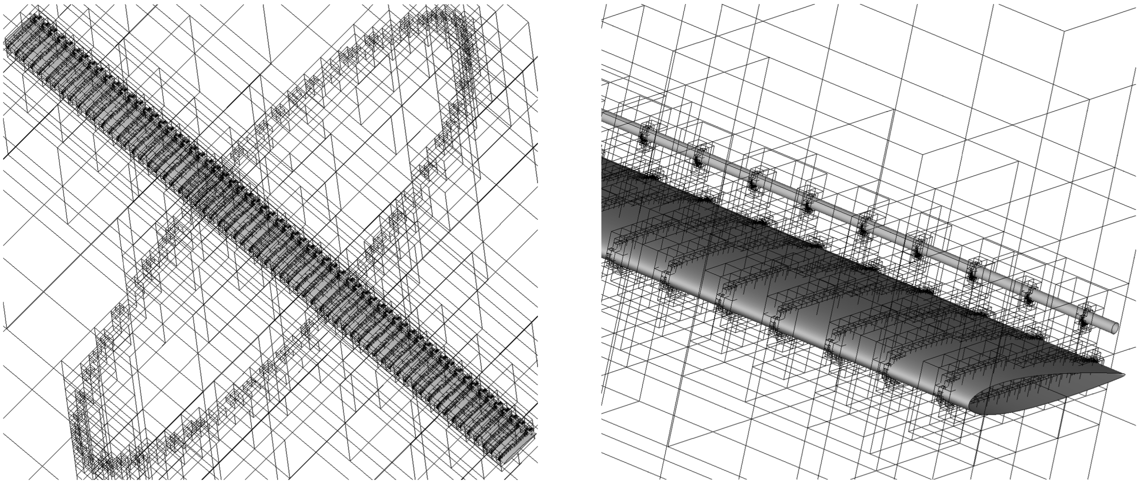

a) 3-D view of computational box

b) 3-D detail of refined dipole source region

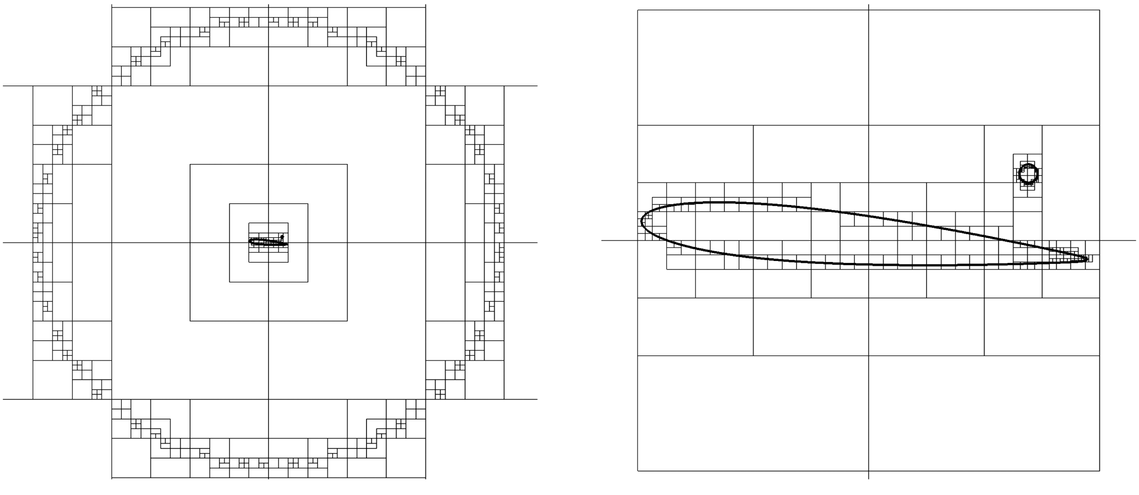

c) 2-D view of computational box

d) 2-D detail of refined dipole source region

Fig. 1 Adaptive refinement of the FMM along regions containing acoustic sources and observer locations.

$$D(\mathbf{oX}, \mathbf{K}) = \sum_{n=0}^{\infty} i^n (2n+1) h_n^{(2)}(K|\mathbf{oX}|) P_n(\mathbf{K}/|\mathbf{K}| \cdot \mathbf{oX}/|\mathbf{oX}|) \tag{6}$$

In the partial-wave expansion method, Green's function from Eq. (3) is written as

$$G(\mathbf{X}, \mathbf{Y}) = \frac{iK}{4\pi} e^{iMK(X_1 - Y_1)} \sum_{n=0}^{\infty} (2n+1) \sum_{m=-n}^{n} S_n^m(\mathbf{oX}) \bar{R}_n^m(\mathbf{oY}) \tag{7}$$

where the singular S^n and regular operators R^n are defined as

$$S_n^m(\mathbf{oX}) = \sqrt{\frac{(n-m)!}{(n+m)!}} h_n^{(2)}(KR) P_n^m(\cos\theta) e^{im\phi} \tag{8}$$

and

$$R_n^m(\mathbf{oY}) = \sqrt{\frac{(n-m)!}{(n+m)!}} j_n(KR) P_n^m(\cos\theta) e^{im\phi} \tag{9}$$

In these expressions, $\mathbf{o}$ is the center of a multipole expansion close to the source location at $\mathbf{Y}$; $h_n^{(2)}$ and j_n stand for the nth-order spherical Hankel function of the second kind and the spherical Bessel function of the first kind, respectively; P_n^m and P_n stand for the associated Legendre polynomials and Legendre polynomials, respectively; $\mathbf{K}$ is the vector of plane-wave samples along the unit sphere surface; $\oint \mathrm{d}(\mathbf{K}/|\mathbf{K}|)$ represents the integral over the unit sphere (see [6–8] for details); the terms R, θ, and ϕ represent the spherical coordinates of some vector, for instance, $\mathbf{oY}$ or $\mathbf{oX}$; and $\bar{(\,)}$ denotes the complex conjugate.

In both formulations, the number of terms used in the functions S, R, and D and the number of plane-wave samples along the unit sphere have to be truncated. The number of truncation terms and plane-wave samples depends on the refinement level and is given by the formula $\varphi_{\mathrm{lv}} = \lfloor k a_{\mathrm{lv}} + c \log(k a_{\mathrm{lv}} + \pi) \rfloor$ [7], where $\lfloor \cdot \rfloor$ stands for the integer part, a_{lv} is the box size at refinement level lv, and the constant c controls the desired accuracy of the solution. Note that results obtained by the FMM-FWH formulation are identical to those obtained by the conventional FWH equation. Both methods depend on the accuracy of the quadrature formulas employed and differences between solutions are controlled by the error tolerance factor c in the FMM. The acceleration obtained with the FMM depends directly on this factor. The choice of a particular value for c depends on the accuracy desired in the FMM calculations. In the present calculations, this constant is chosen as $c = 8$, which provided errors smaller than those from the numerical integrations. The authors suggest the papers from Darve [22], Song and Chew [23], and Gumerov and Duraiswami [11] for details regarding the accuracy of the FMM and the choice of constant c. Also note that the acceleration of the FMM also depends on the number of levels of refinement and on the spatial distribution of observer and source locations. Applying the partial-wave expansion and plane-wave expansion formulations to the FWH equation, one can write multipole expansions as

$$M_n^m(\mathbf{o}) = \int_{f=0} \hat{F}_i \frac{\partial(\bar{R}_n^m(\mathbf{oY}) e^{-iMKY_1})}{\partial Y_l} \frac{\partial Y_l}{\partial y_i} \,\mathrm{d}S + \int_{f>0} \hat{T}_{ij} \frac{\partial^2(\bar{R}_n^m(\mathbf{oY}) e^{-iMKY_1})}{\partial Y_l \partial Y_q} \frac{\partial Y_l}{\partial y_j} \frac{\partial Y_q}{\partial y_i} \,\mathrm{d}V \tag{10}$$

and

$$M(\mathbf{o}, \mathbf{K}) = \int_{f=0} \hat{F}_i \frac{\partial(I(\mathbf{oY}, \mathbf{K}) e^{-iMKY_1})}{\partial Y_l} \frac{\partial Y_l}{\partial y_i} \,\mathrm{d}S + \int_{f>0} \hat{T}_{ij} \frac{\partial^2(I(\mathbf{oY}, \mathbf{K}) e^{-iMKY_1})}{\partial Y_l \partial Y_q} \frac{\partial Y_l}{\partial y_j} \frac{\partial Y_q}{\partial y_i} \,\mathrm{d}V \tag{11}$$

respectively. Details about the implementation of the 3-D wideband FMM, including the conversion of multipole expansions to local expansions and the translation of multipole/local expansions to multipole/local expansions at different levels of adaptive refinement, can be found in [6]. Calculations of the acoustic pressure can be performed by

$$\begin{aligned}[\hat{p}' H(f)] = {} & \left[-\int_{f=0} \hat{F}_i(\mathbf{y}) \frac{\partial G(\mathbf{x}, \mathbf{y})}{\partial y_i} \,\mathrm{d}S - \int_{f>0} \hat{T}_{ij} H(f) \frac{\partial^2 G(\mathbf{x}, \mathbf{y})}{\partial y_i \partial y_j} \,\mathrm{d}V \right]_{\mathrm{FWH}} \\ & + \left\{ \frac{ik}{4\pi} \left[\frac{1}{4\pi} \oint e^{i\mathbf{K}\cdot\mathbf{oX}} e^{iMKX_1} L(\mathbf{o}, \mathbf{K}) \,\mathrm{d}(\mathbf{K}/|\mathbf{K}|) + \sum_{n=0}^{\varphi_{\mathrm{lv}}} (2n+1) \sum_{m=-n}^{n} e^{iMKX_1} R_n^m(\mathbf{oX}) L_n^m(\mathbf{o}) \right] \right\}_{\mathrm{FMM}}\end{aligned} \tag{12}$$

where the terms with subscript FWH represent nearby calculations among sources and observer locations, and those with subscript FMM represent distant calculations. The criteria used for deciding between nearby and distant calculations follow that of the multilevel adaptive FMM described in the literature [20]. At any level, if two sets of elements are well separated, computations among sources and observers are performed by the FMM-FWH method. Otherwise, the conventional FWH method is used. In the expression above, $\mathbf{o}$ is the center of a local expansion close to the observer location at $\mathbf{X}$. The terms $L_n^m(\mathbf{o})$ and $L(\mathbf{o}, \mathbf{K})$ are the local expansions computed through the partial-wave expansion and plane-wave expansion formulations, respectively. A full description of these terms can be found in [6].

V. Results

This section discusses results obtained by direct calculation and the FMM-FWH formulation. The sound generated by the unsteady flow past a cylinder in the proximity of a NACA0012 airfoil is studied and the interaction of both geometries is analyzed for different cylinder positions. A summary of the configurations studied is presented in Table 1. The developed numerical capability allows the analysis of each sound source individually. Therefore, the effects of dipoles and quadrupoles for each configuration are investigated. The method can also be applied for a porous FWH surface, and results will show that large acceleration factors are obtained by the FMM-FWH formulation, even if only surface sources are considered. However, in this work we want to investigate the effects of each sound source individually, including surface sources for each configuration, plus volume sources. This type of simulation is relevant for acoustic predictions of airframe noise configurations such as landing gears and high-lift devices. Using the porous FWH surface it would not be possible to identify the contribution of sound generation of each individual source.

An assessment in terms of computational cost of the FMM-FWH and conventional FWH formulations is presented. The solutions are shown in terms of directivity plots, 2-D field plots, and spherical directivity plots. Convection effects on dipole and quadrupole source integrations are assessed. A grid refinement study is performed in order to ensure that the unsteady flow solutions are converged and only results obtained for the most refined grids are discussed. For the direct calculation, two overset O-grids are used along the boundary-layer regions of the NACA0012 and cylinder and a background O-grid is used to capture the wake regions and acoustic field. The NACA0012 boundary-layer grid has 400 × 60 grid points, the cylinder boundary-layer grid has 240 × 45 grid points, and the

Table 1 Summary of cylinder and NACA0012 airfoil configurations analyzed

Vortex-shedding frequency analyzed	Position of center of cylinder[a]
Case 1, cylinder	$x = 0.85$ and $y = 0.15$
Case 2, NACA0012	$x = 0.85$ and $y = 0.30$
Case 3, cylinder	$x = 0.85$ and $y = 0.30$

[a] The airfoil leading edge is at $x = 0.0$ and $y = 0.0$.

background grid has 400 × 625 grid points,and the far-field location is at $25c$, where c is the airfoil chord. Direct and acoustic calculations are performed by a cluster computer with 2.33 GHz Intel Xeon CPUs and 8 GB of memory per node. The unsteady flows and the acoustic fields generated by the flows are performed by 2-D direct calculations. To verify the solution obtained by the 3-D FMM-FWH formulation, the surface dipole and volume quadrupole sources are extruded in the spanwise direction to form rectangular surfaces (dipoles) and hexahedral volumes (quadrupoles). The magnitude and phase of the 3-D source terms are set constant along the span elements, and the span extent is increased until convergence of the acoustic solution is achieved. The span size used for cases 1 and 3 is $15c$ and that used for case 2 is $35c$. Finally, the 3-D solutions obtained by the FMM-FWH formulation for a plane passing through the middle span are compared with those obtained by the 2-D direct calculations in terms of directivity and field plots. For all cases analyzed, 64 surface and volume elements are used along the spanwise direction in order to obtain accurate solutions for the FMM-FWH formulation. Therefore, the total number of dipole terms for the configurations analyzed is 40,960, and the total number of quadrupole source terms is 12,224,000.

A. Case 1: Cylinder Vortex-Shedding Frequency

In the first problem, sound generated by the unsteady flow past a NACA0012 airfoil with rounded trailing edge and a cylinder located close to its trailing-edge boundary-layer region is studied. The configuration is at an angle of attack of $\alpha = 5$ deg. and the Mach number is $M = 0.3$. The Reynolds number based on the airfoil chord is $Re = 5000$, and the Reynolds number based on the diameter of the cylinder is $Re = 200$. In the paper by Singer et al. [24], a similar configuration composed of an airfoil plus a bluff-body vortex generator is studied. However, that study addressed the scattering of vortices generated by artificial viscosity past the bluff body and convected through the sharp trailing edge. In this study, the scattering of sound generated by the cylinder wake on the airfoil surface is analyzed. Since the geometries are closely located, there is a boundary-layer interaction and no vortex shedding is observed for the NACA0012 airfoil.

The vorticity field and the aerodynamic forces around the airfoil and cylinder are shown in Fig. 2. Note that the unsteady lift generated by the airfoil and cylinder are at the same frequency and have comparable oscillation amplitudes. However, the airfoil shows a positive lift mean value and the cylinder shows a small negative lift mean value, due to the flow acceleration between the geometries. One can also see in the figure that there is a phase difference between the unsteady aerodynamic forces generated on both geometries. This will play an important role in the sound generated by this configuration. The Strouhal number obtained for the cylinder vortex-shedding frequency is $St = f2R/U = 0.19$ based on the cylinder diameter. Here, the nondimensional velocity $U = 0.3$ and the nondimensional frequency $f = 1.33$. Figure 3 shows the directivity

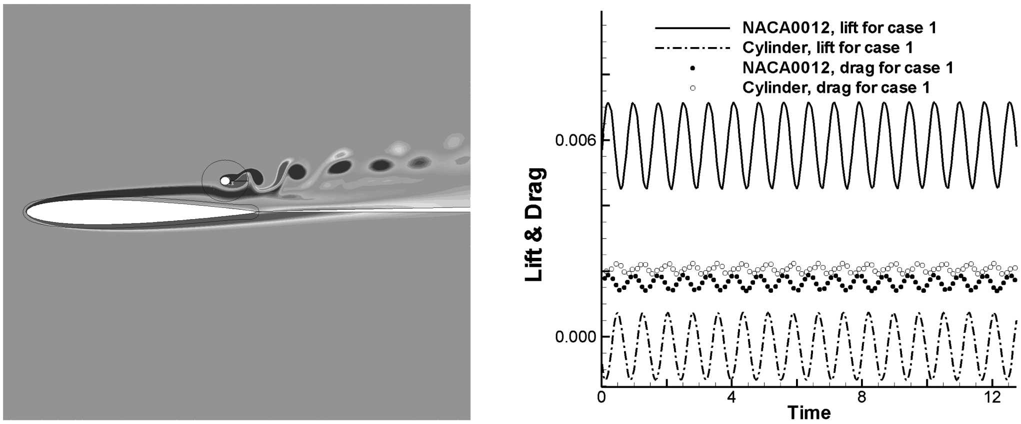

a) Vorticity field
b) Aerodynamic forces

Fig. 2 Case 1: cylinder in the proximity of NACA0012 airfoil.

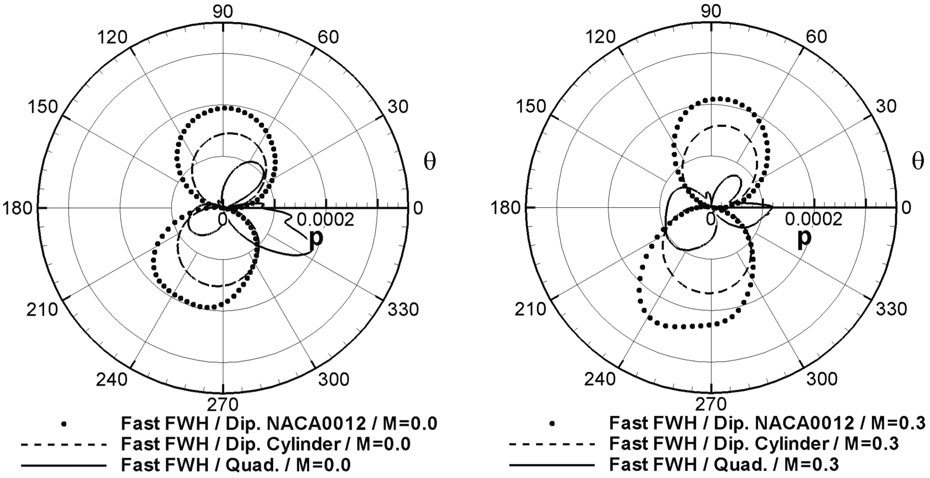

a) Neglecting convection effects
b) Including convection effects

Fig. 3 Directivity plot for the individual noise sources at the cylinder vortex-shedding frequency (case 1) for observer locations at $6c$ distant from the NACA0012 airfoil midchord.

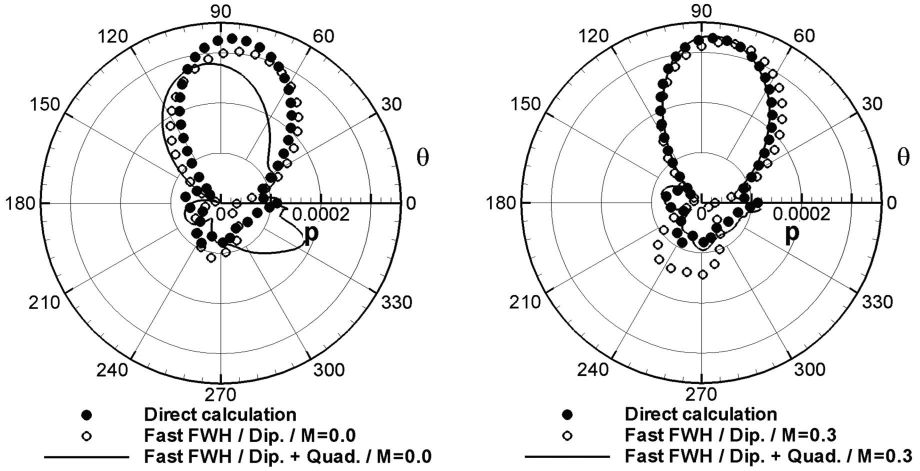

a) Neglecting convection effects **b) Including convection effects**

Fig. 4 Directivity plot for the cylinder vortex-shedding frequency (case 1) for observer locations at 6*c* distant from the NACA0012 airfoil midchord.

plots for the individual noise sources at the cylinder vortex-shedding frequency for observer locations at $6c$, which corresponds to ≈ 8 acoustic wavelengths. The convection effects observed in the figures affect the magnitude and directivity of the dipole source terms, especially those associated with the NACA0012 airfoil. However, the main convection effects are shown in the quadrupole source terms. Figures 4–6 show directivity plots for observer locations at $6c$, 2-D field plots, and spherical directivity plots for observer locations at $9c$, respectively, for the cylinder vortex-shedding frequency. Results are presented for the direct calculation (polar and 2-D field plots) and FMM-FWH formulation, including effects of convection and quadrupole sources.

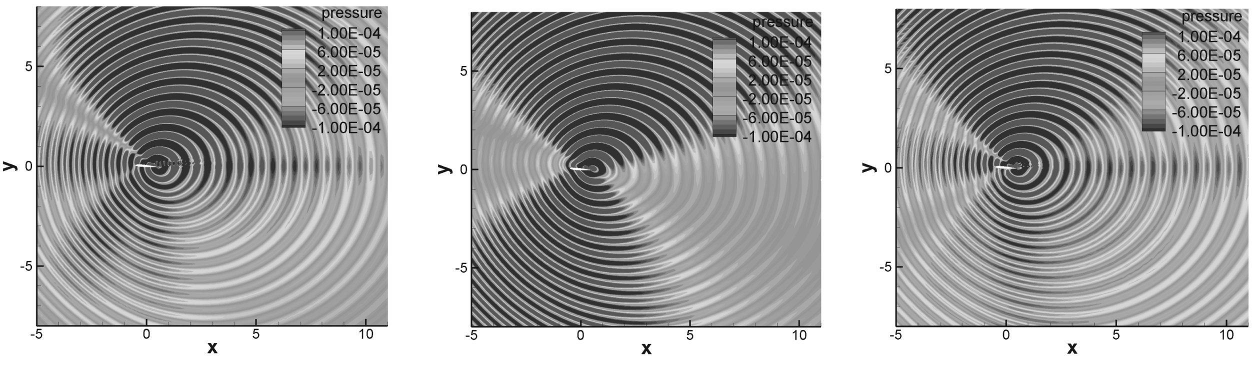

a) Direct calculation **b) FMM-FWH formulation: dipoles with convection at $M = 0.3$** **c) FMM-FWH formulation: dipoles + quadrupoles with convection at $M = 0.3$**

Fig. 5 Acoustic field for the cylinder vortex-shedding frequency (case 1).

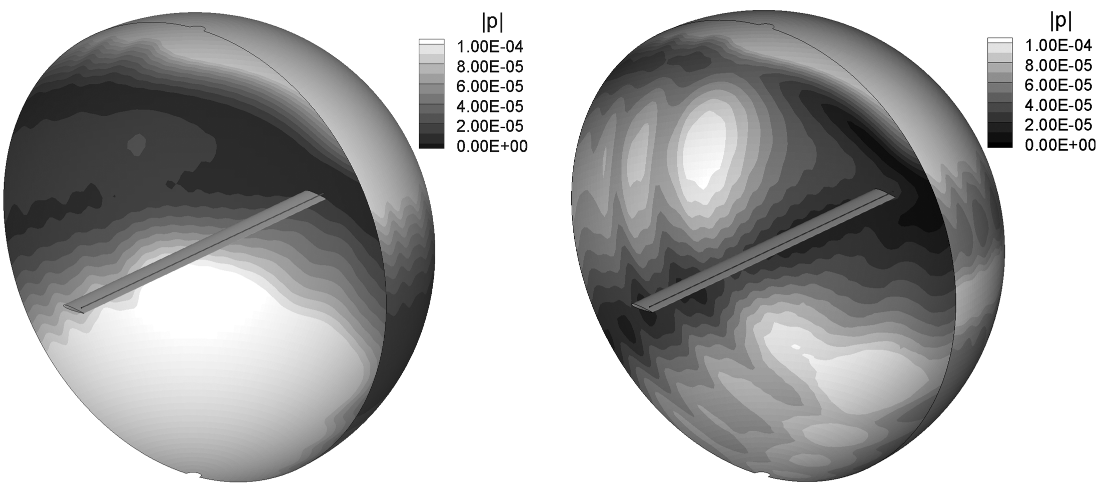

a) Neglecting convection effects **b) Including convection effects**

Fig. 6 Spherical directivity plot for the cylinder vortex-shedding frequency (case 1) for observer locations at 9*c* distant from the NACA0012 airfoil midchord.

Table 2 Computational cost (in seconds) and cost-reduction factor for case 1

	Directivity plot	2-D field plot	3-D directivity plot
Dipoles, FWH	64	2,995	1,586
Dipoles, FMM-FWH	24	43	52
Cost-reduction factor	2.7	69.7	30.5
Dipoles plus quadrupoles, FWH	5,363	252,977	127,170
Dipoles plus quadrupoles, FMM-FWH	1,180	1,741	1,398
Cost-reduction factor	4.5	145.3	86.6

As shown in Figs. 4–6, this configuration shows a complex directivity pattern for the cylinder vortex-shedding frequency, due to the interaction of sound sources. Sound is radiated toward the top region of the airfoil, due to scattering along the airfoil surface. Radiation in the upstream and downstream directions is due solely to quadrupole sources and sound radiated in the region below the airfoil occurs from the combination of dipole radiation due to unsteady forces on the airfoil and cylinder and radiation due to quadrupole sources. When convective effects and quadrupole source terms are included, the solution obtained by the hybrid method shows good agreement with the direct calculation, as shown in Figs. 4b and 5c.

The directivity plots in Fig. 4 are obtained by the FMM-FWH formulation in 24 and 1180 s for calculations including dipoles and dipoles plus quadrupoles, respectively. The computational time for directivity plots obtained through the conventional solution of the FWH formulation is 64 and 5363 s for calculations including dipoles and dipoles plus quadrupoles, respectively. Therefore, factors of 2.7 and 4.5 in computational cost reduction are observed. The cost-reduction factors for the 3-D solutions are smaller than with the 2-D results from [4]. This is a consequence of the more expensive preprocessing steps. For all simulations presented in this work the adaptive refinement step is precomputed and stored. This procedure is useful for multifrequency analysis, such as in the study of airframe noise configurations.

The 2-D field solutions shown in Fig. 5 are obtained by the FMM-FWH formulation for an acoustic grid with 180×180 observer locations in 43 and 1741 s for calculations including dipoles and dipoles plus quadrupoles, respectively. The computational time for directivity plots obtained through the conventional solution of the FWH formulation is 2995 and 252,977 s for calculations including dipoles and dipoles plus quadrupoles, respectively. Therefore, factors of 69.7 and 145.3 in computational cost reduction are observed.

Finally, the 3-D directivity mapping solutions shown in Fig. 6 are obtained by the FMM-FWH formulation for an acoustic grid with 180×90 observer locations in 52 and 1398 s for calculations including dipoles and dipoles plus quadrupoles, respectively. The computational time for directivity plots obtained through the conventional solution of the FWH formulation is 1586 and 121,100 s for calculations including dipoles and dipoles plus quadrupoles, respectively. Therefore, factors of 30.5 and 86.6 in computational cost reduction are observed. A comparison of computational cost for the first case studied is summarized in Table 2. Almost all the computational cost for the FMM-FWH method comes from the multipole calculations. This cost is independent of the number of observer locations and is related to the number of noise sources. This explains the better performance for the solution of 2-D field plots and spherical directivity plots, compared with that obtained for the solution of directivity plots.

B. Case 2: NACA0012 Vortex-Shedding Frequency

In this case, the cylinder is moved away from the airfoil boundary-layer region. Again, the configuration is at an angle of attack of $\alpha = 5$ deg and the Mach number is $M = 0.3$. The Reynolds number based on the airfoil chord is $Re = 5000$ and the Reynolds number based on the diameter of the cylinder is $Re = 200$. For this configuration, vortex shedding is observed for both the NACA0012 airfoil and cylinder. In this case, we analyze the sound generated at the airfoil vortex-shedding frequency. The vorticity field and the aerodynamic forces around the airfoil and cylinder are shown in Fig. 7. One can see that the unsteady lift produced by the airfoil is affected by the presence of the cylinder and is therefore composed of the vortex-shedding frequencies of both geometries. The unsteady lift produced by the cylinder shows only the effect of the cylinder vortex-shedding frequency. Again, the cylinder lift mean value is negative, due to the flow acceleration between the geometries. For this configuration, the phase difference between the unsteady forces is small, compared with that shown in case 1.

The Strouhal number obtained for the airfoil vortex-shedding frequency is $St = fc/U = 1.80$ based on the airfoil chord length. Here, the nondimensional velocity $U = 0.3$ and the nondimensional frequency $f = 0.54$.

Figure 8 shows the directivity plots for the individual noise sources for the airfoil vortex-shedding frequency for observer locations at $12c$, which corresponds to ≈ 6 acoustic wavelengths. The magnitude of the cylinder dipoles is negligible for this frequency and is therefore not shown. Convection effects considerably affect the magnitude of the dipole source terms and the magnitude and directivity of quadrupole source terms. Figures 9–11 show directivity plots for

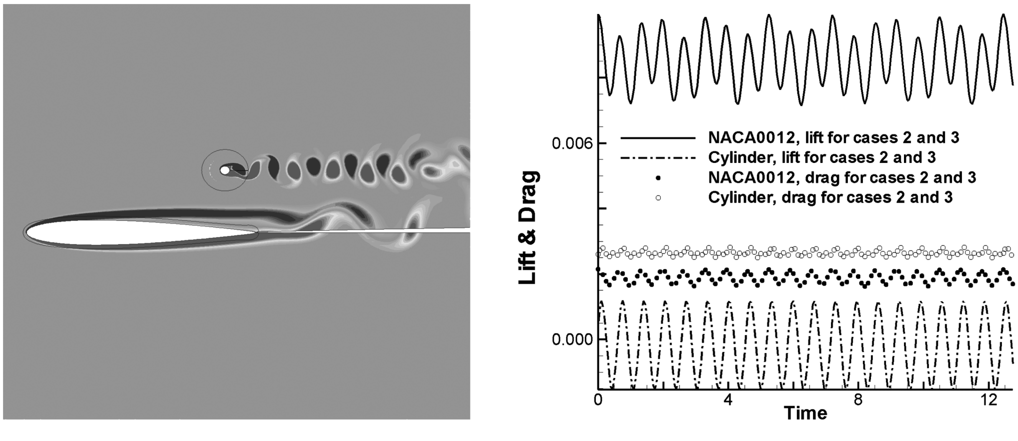

a) Vorticity field b) Aerodynamic forces

Fig. 7 Cases 2 and 3: cylinder in the proximity of NACA0012 airfoil.

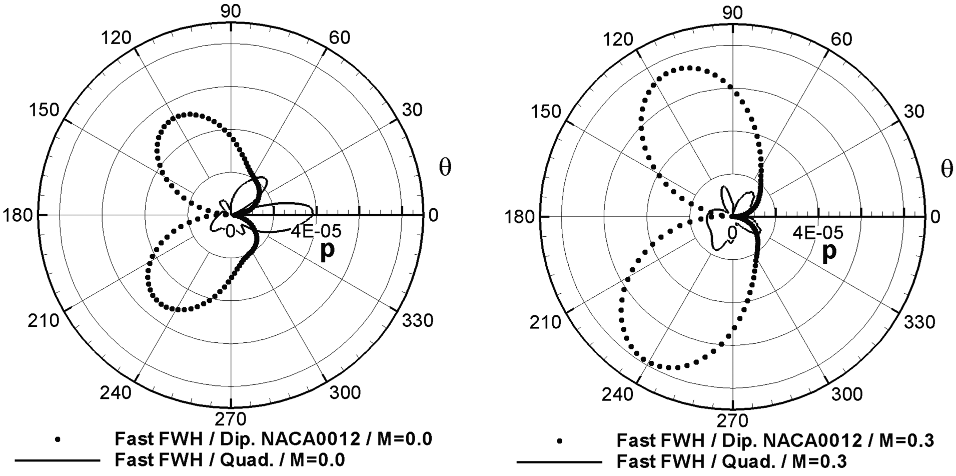

a) Neglecting convection effects b) Including convection effects

Fig. 8 Directivity plot for the individual noise sources at the airfoil vortex-shedding frequency (case 2) for observer locations at 12*c* distant from the NACA0012 airfoil midchord.

observer locations at 12c, 2-D field plots, and spherical directivity plots for observer locations at 35c, respectively, for the airfoil vortex-shedding frequency. Results are presented for the direct calculation (polar and 2-D field plots) and FMM-FWH formulation, including effects of convection and quadrupole sources. As shown in the figures, sound radiated at this frequency presents a directivity pattern similar to that of a single airfoil [4] with two main lobes directed upstream. Quadrupole effects mainly affect the magnitude of the directivity and convection effects are important, since they considerably modify the sound directivity. The solution obtained by the hybrid method shows good agreement with the direct calculation, as shown in Figs. 9b and 10c. A comparison of computational cost for the second case studied is summarized in Table 3. Note that factors of computational cost reduction are larger for this case, because the

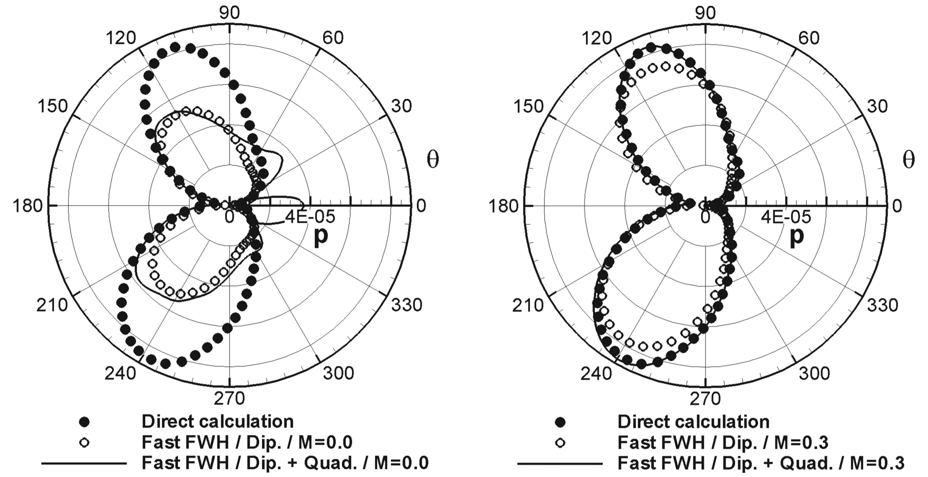

a) Neglecting convection effects b) Including convection effects

Fig. 9 Directivity plot for the airfoil vortex-shedding frequency (case 2) for observer locations at 12*c* distant from the NACA0012 airfoil midchord.

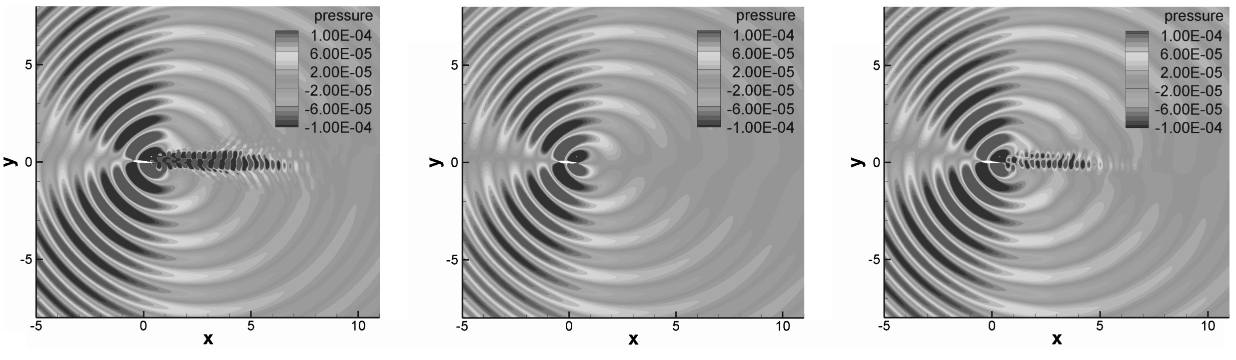

a) Direct calculation

b) FMM-FWH formulation: dipoles with convection at $M = 0.3$.

c) FMM-FWH formulation: dipoles + quadrupoles with convection at $M = 0.3$

Fig. 10 Acoustic field for the airfoil vortex-shedding frequency (case 2).

Table 3 Computational cost (in seconds) and cost-reduction factor for case 2

	Directivity plot	2-D field plot	3-D directivity plot
Dipoles, FWH	64	2,996	1,588
Dipoles, FMM-FWH	18	26	46
Cost-reduction factor	3.6	115.2	34.5
Dipoles plus quadrupoles, FWH	5,365	253,300	127,170
Dipoles plus quadrupoles, FMM-FWH	756	1,236	858
Cost-reduction factor	7.1	204.9	148.2

NACA0012 vortex-shedding frequency is smaller than that for the cylinder in case 1. The 2-D field solutions shown in Fig. 10 and the 3-D directivity mapping solutions shown in Fig. 11 are obtained by the FMM-FWH formulation for acoustic grids with 180 × 180 and 180 × 90 observer locations, respectively.

C. Case 3: Cylinder Vortex-Shedding Frequency

Sound generated by the configuration from case 2 at the cylinder vortex-shedding frequency is analyzed in case 3. The Strouhal number obtained for the vortex-shedding frequency is $St = f2R/U = 0.2$ based on the cylinder diameter. Here, the nondimensional velocity $U = 0.3$ and the nondimensional frequency is $f = 1.49$. Figure 12 shows the directivity plots for the individual sound sources for the cylinder vortex-shedding frequency for observer locations at $5c$, which corresponds to ≈ 7.5 acoustic wavelengths. Convection effects affect the magnitude and directivity of the airfoil dipole sources and directivity of quadrupole sources. Figures 13–15 show directivity plots for observer locations at $5c$, 2-D field plots, and spherical directivity plots for observer locations at $15c$, respectively, for the cylinder vortex-shedding frequency. Results are presented for the direct calculation (polar and 2-D field plots) and FMM-FWH formulation including effects of convection and quadrupole sources.

In the directivity plots from Fig. 13, note that the amplitude of acoustic pressure at this frequency is larger (by almost 1 order of

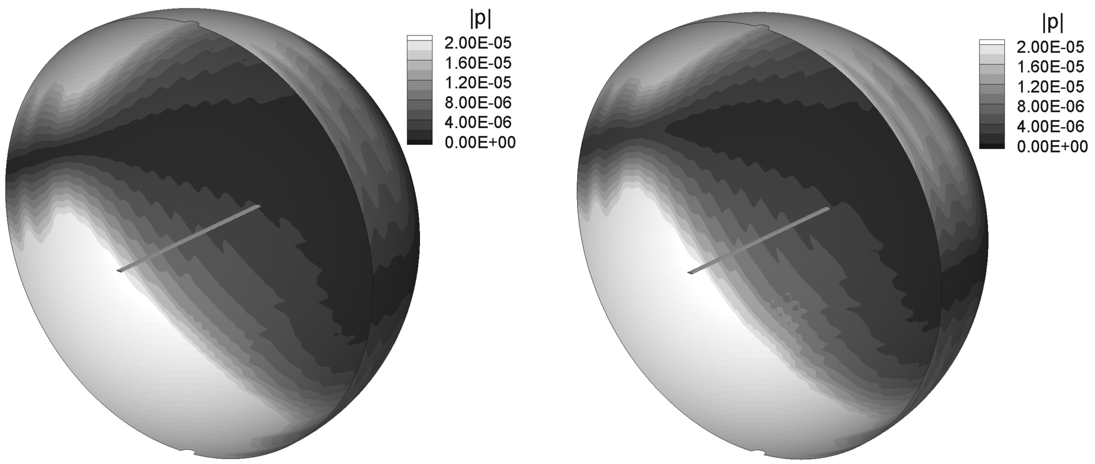

a) Neglecting convection effects b) Including convection effects

Fig. 11 Spherical directivity plot for the airfoil vortex-shedding frequency (case 2) for an observer location at 35*c* distant from the NACA0012 airfoil midchord.

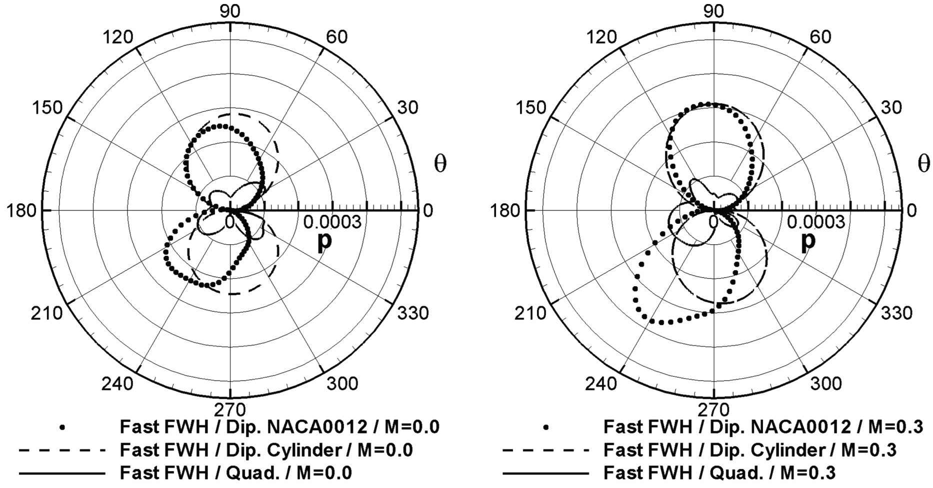

a) Neglecting convection effects b) Including convection effects

Fig. 12 Directivity plot for the individual noise sources at the cylinder vortex-shedding frequency (case 3) for observer locations at 5*c* distant from the NACA0012 airfoil midchord.

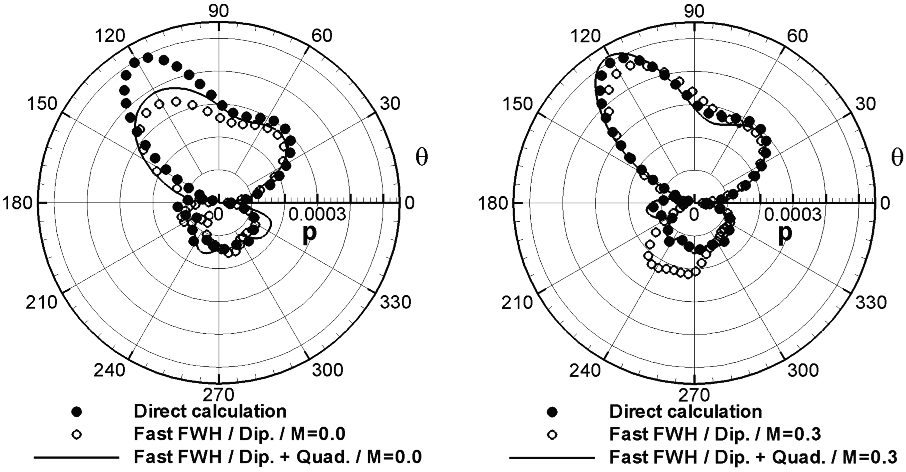

a) Neglecting convection effects **b) Including convection effects**

Fig. 13 Directivity plot for the cylinder vortex-shedding frequency (case 3) for observer locations at 5*c* distant from the NACA0012 airfoil midchord.

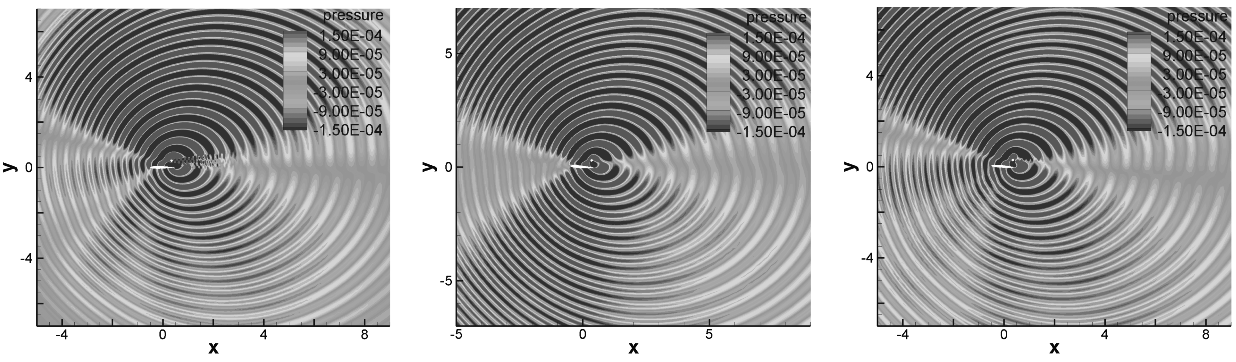

a) Direct calculation

b) FMM-FWH formulation: dipoles with convection at *M* = 0.3

c) FMM-FWH formulation: dipoles + quadrupoles with convection at *M* = 0.3

Fig. 14 Acoustic field for the cylinder vortex-shedding frequency (case 3).

magnitude) than that shown at the airfoil vortex-shedding frequency. As shown in Figs. 13–15, this configuration shows a complex directivity pattern, due to the interaction of the sound sources. Sound is radiated toward the top region of the airfoil in a bean-shaped directivity, due to a combination of dipole radiation (unsteady forces on the airfoil and cylinder) and quadrupole radiation. Radiation in the upstream direction is due solely to quadrupole sources and sound radiated in the region below the airfoil occurs from the interaction of radiation, due to dipole and quadrupole sources. When convective effects and quadrupole source terms are included, the solution obtained by the hybrid method shows good agreement with the direct calculation, as shown in Figs. 13b and 14c. Comparing the directivity solutions for the cylinder vortex-shedding frequencies shown in Fig. 4b for case 1 and Fig. 13b for case 3, note that the cylinder position plays an important role in the flow and, therefore, in the acoustic solutions. For case 1, sound is radiated toward 90 deg along

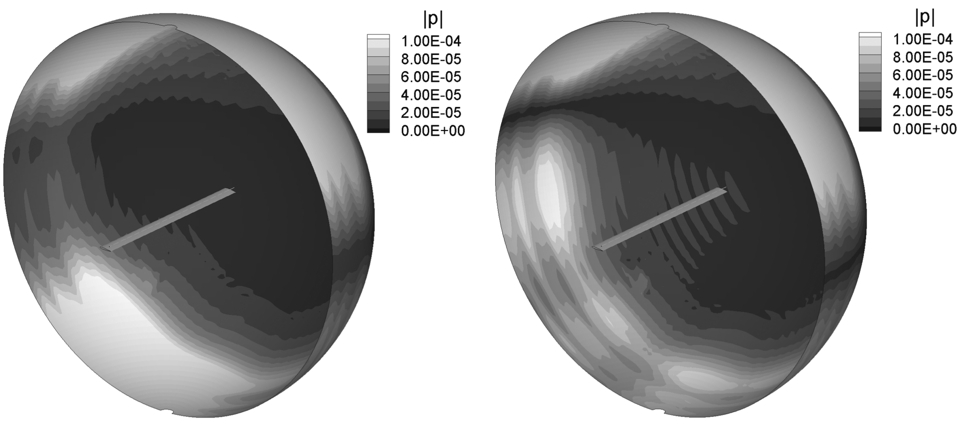

a) Neglecting convection effects **b) Including convection effects**

Fig. 15 Spherical directivity plot for the cylinder vortex-shedding frequency (case 3) for observer locations at 15*c* distant from the NACA0012 airfoil midchord.

Table 4 Computational cost (in seconds) and cost-reduction factor for case 3

	Directivity plot	2-D field plot	3-D directivity plot
Dipoles, FWH	64	2,999	1,590
Dipoles, FMM-FWH	23	45	56
Cost-reduction factor	2.8	66.6	28.4
Dipoles plus quadrupoles, FWH	5,388	253,700	127,900
Dipoles plus quadrupoles, FMM-FWH	1,434	2,280	2,234
Cost-reduction factor	3.8	111.3	57.3

the top region of the airfoil, and for case 3, sound is radiated in a bean-shaped directivity, mainly at 120 deg upstream and at 45 deg downstream.

A comparison of computational cost for the third case studied is summarized in Table 4. For case 3, the factors of computational cost reduction are slightly smaller than those obtained for case 1. This is a consequence of the higher cylinder vortex-shedding frequency for this case. Again, the 2-D field solutions shown in Fig. 14 and the 3-D directivity mapping solutions shown in Fig. 15 are obtained by the FMM-FWH formulation for acoustic grids with 180×180 and 180×90 observer locations, respectively. Also note that the 3-D directivity mapping solutions for this case are obtained for observer locations at a larger far-field distance than that shown in case 1. Therefore, calculations are performed by the FMM-FWH formulation for higher local Helmholtz numbers.

VI. Conclusions

In the present work, a hybrid method is used to predict the sound generated by unsteady flows past a cylinder in the proximity of a NACA0012 airfoil. Different cylinder positions are considered in order to analyze the interaction effects between the geometries. In the current hybrid method, near-field flow quantities are obtained by direct calculation and far-field sound radiation is computed by the Ffowcs Williams–Hawkings (FWH) equation. A 3-D wideband multilevel adaptive fast multipole method (FMM) is implemented in order to reduce the computational cost of field solutions with many observer locations. The numerical method is described for the solution of a 3-D Green's function that incorporates convective effects. The surface integrations appearing in the FWH equation are computed along the scattering body surfaces and the volume integrations are computed along a subset region of the flowfield, including the wake-plus-boundary-layer regions. The developed numerical capability allows the analysis of the individual noise sources and the investigation of the effects of dipoles and quadrupoles for each configuration.

The solutions obtained by the 3-D FMM-FWH method are compared with 2-D direct calculations and results are in good agreement. It is observed that the position of the cylinder considerably affects aerodynamic and aeroacoustic solutions. In the first configuration analyzed, the cylinder is closer to the airfoil and only cylinder vortex shedding is observed. In the second configuration, the cylinder is displaced further away from the airfoil and vortex shedding is observed for both geometries. A comparison at the cylinder vortex-shedding frequency shows large differences for directivity of acoustic pressure for the configurations analyzed. The solutions are also presented in terms of 2-D field plots and spherical directivity plots and an assessment in terms of computational cost of the FMM-FWH and conventional FWH formulations is presented. Results obtained by the FMM-FWH method are up to 2 orders of magnitude faster than with the conventional computation of FWH equation. The study of sound generation by flows past complex configurations such as landing gears and high-lift devices, where wakes and shear layers have important contributions to noise generation, can benefit from the method presented here.

Acknowledgment

The authors acknowledge the support of Fulbright and Coordination for Improvement of Higher Education Personnel (CAPES) through a Ph.D. Scholarship for the first author under the Fulbright/CAPES grant no. 2464055.

References

[1] Lyrintzis, A. S., "Surface Integral Methods in Computational Aeroacoustics—From the (CFD) Near Field to the (Acoustic) Far Field," *International Journal of Aeroacoustics*, Vol. 2, 2003, pp. 95–128.
doi:10.1260/147547203322775498

[2] Freund, J. B., "A Simple Method for Computing Far-Field Sound in Aeroacoustic Computations," *Journal of Computational Physics*, Vol. 157, 2000, pp. 796–800.
doi:10.1006/jcph.1999.6392

[3] Margnat, F., "A Fast Procedure for the Computation of Acoustic Fields Given by Retarded-Potential Integrals," Proceedings of the 16th AIAA/CEAS Aeroacoustics Conference, AIAA Paper 2010-3708, 2010, pp. 1–10.

[4] Wolf, W. R., and Lele, S. K., "Acoustic Analogy Formulations Accelerated by Fast Multipole Method for Two-Dimensional Aeroacoustic Problems," *AIAA Journal*, Vol. 48, 2010, pp. 2274–2285.
doi:10.2514/1.J050338

[5] Lockard, D. P., "A Comparison of Ffowcs Williams–Hawkings Solvers for Airframe Noise Applications," *Proceedings of the 8th AIAA/CEAS Aeroacoustics Conference*, AIAA Paper 2002-2580, 2002, pp. 1–11.

[6] Wolf, W. R., and Lele, S. K., "Wideband Fast Multipole Boundary Element Method: Application to Acoustic Scattering from Aerodynamics Bodies," *International Journal for Numerical Methods in Fluids* (accepted for publication).

[7] Coifman, R., Rokhlin, V., and Wandzura, S., "The Fast Multipole Method for the Wave Equation: A Pedestrian Prescription," *IEEE Antennas and Propagation Magazine*, Vol. 35, No. 3, 1993, pp. 7–12.
doi:10.1109/74.250128

[8] Sakuma, T., and Yasuda, Y., "Fast Multipole Boundary Element Method for Large-Scale Steady-State Sound Field Analysis. Part I: Setup and Validation," *Acta Acustica*, Vol. 88, 2002, pp. 513–525.

[9] Jakob-Chien, R., and Alpert, B. K., "A Fast Spherical Filter with Uniform Resolution," *Journal of Computational Physics*, Vol. 136, 1997, pp. 580–584.
doi:10.1006/jcph.1997.5782

[10] Shen, L., and Liu, Y. J., "An Adaptive Fast Multipole Boundary Element Method for Three-Dimensional Acoustic Wave Problems based on the Burton-Miller Formulation," *Computational Mechanics*, Vol. 40, 2007, pp. 461–472.
doi:10.1007/s00466-006-0121-2

[11] Gumerov, N. A., and Duraiswami, R., "A Broadband Fast Multipole Accelerated Boundary Element Method for the Three-Dimensional Helmholtz Equation," *Journal of the Acoustical Society of America*, Vol. 125, 2009, pp. 191–205.
doi:10.1121/1.3021297

[12] Howe, M. S., *Acoustics of Fluid-Structure Interactions*, Cambridge Univ. Press, Cambridge, England, U.K., 1998.

[13] Nagarajan, S., Lele, S. K., and Ferziger, J. H., "A Robust High-Order Method for Large Eddy Simulation," *Journal of Computational Physics*, Vol. 191, 2003, pp. 392–419.
doi:10.1016/S0021-9991(03)00322-X

[14] Bhaskaran, R., and Lele, S. K., "Large Eddy Simulation of Free-Stream Turbulence Effects on Heat Transfer to a High-Pressure Turbine Cascade," *Journal of Turbulence*, Vol. 11, 2010, pp. 1–15.

[15] Beam, R. M., and Warming, R. F., "An Implicit Factored Scheme for the Compressible Navier-Stokes Equations," *AIAA Journal*, Vol. 16, 1978, pp. 393–402.
doi:10.2514/3.60901

[16] Nagarajan, S., "Leading Edge Effects in Bypass Transition," Ph.D. Thesis, Stanford University, 2004.

[17] Ffowcs Williams, J. E., and Hawkings, D. L., "Sound Generation by Turbulence and Surface in Arbitrary Motion," *Philosophical*

Transactions of the Royal Society of London, Series A: Mathematical and Physical Sciences, Vol. 264, 1969, pp. 321–342.
doi:10.1098/rsta.1969.0031

[18] Wang, M., Lele, S. K., and Moin, P., "Computation of Quadrupole Noise Using Acoustic Analogy," *AIAA Journal*, Vol. 34, 1996, pp. 2247–2254.
doi:10.2514/3.13387

[19] Casper, J. H., Lockard, D. P., Khorrami, M. R., and Streett, C. L., "Investigation of Volumetric Sources in Airframe Noise Simulations," 10th AIAA/CEAS Aeroacoustics Conference, AIAA Paper 2004-2805, 2004, pp. 1–10.

[20] Nishimura, N., "Fast Multipole Accelerated Boundary Integral Equation Methods," *Applied Mechanics Reviews*, Vol. 55, 2002, pp. 299–324.
doi:10.1115/1.1482087

[21] Dembart, B., and Yip, E., "The Accuracy of Fast Multipole Methods for Maxwell's Equations," *IEEE Computational Science and Engineering*, Vol. 5, No. 3, 1998, pp. 48–56.
doi:10.1109/99.714593

[22] Darve, E., "The Fast Multipole Method I: Error Analysis and Asymptotic Complexity," *SIAM Journal on Numerical Analysis*, Vol. 38, No. 1, 2000, pp. 98–128.
doi:10.1137/S0036142999330379

[23] Song, J. M., and Chew, W. C., "Error Analysis for the Truncation of Multipole Expansion of Vector Green's Functions," *IEEE Microwave and Wireless Components Letters*, Vol. 11, No. 7, 2001, pp. 311–313.
doi:10.1109/7260.933781

[24] Singer, B. A., Brentner, K. S., and Lockard, D. P., "Simulation of Acoustic Scattering from a Trailing Edge," *Journal of Sound and Vibration*, Vol. 230, 2000, pp. 541–560.
doi:10.1006/jsvi.1999.2628

A. Lyrintzis
Associate Editor